Supporting Information

Three-Dimensional Hierarchical Nickel-Cobalt-Sulfide Nanostructures for High Performance Electrochemical Energy Storage Electrodes

Zhenhu Li,[a]   Xu Li,[a,d] Lu Xiang,[a,c] Xiong Xie [a,c] Xue Li,[e] Dong-Rong Xiao,[a,d] Jun Shen,[a,c] Wenqiang Lu, [a] Li Lu [*b] and Shuangyi Liu [*a]

a. Chongqing Key Laboratory of Multi-Scale Manufacturing Technology, Chongqing Institute of Green and Intelligent Technology, Chinese Academy of Sciences, Chongqing 400714, P. R. China

b. Department of Mechanical Engineering, National University of Singapore, Singapore 117576

c. State Key Laboratory of Mechanical Transmission, College of Materials Science and Engineering, Chongqing University, Chongqing 400044, P. R. China

d. College of Chemistry and Chemical Engineering, Southwest University, Chongqing, 400715, PR China

e. Department of Chemical and Biomolecular Engineering, Johns Hopkins University, 3400 North Charles Street, Baltimore MD 21218, USA

* Corresponding author

E-mail: liushuangyi@cigit.ac.cn; luli@nus.edu.sg.
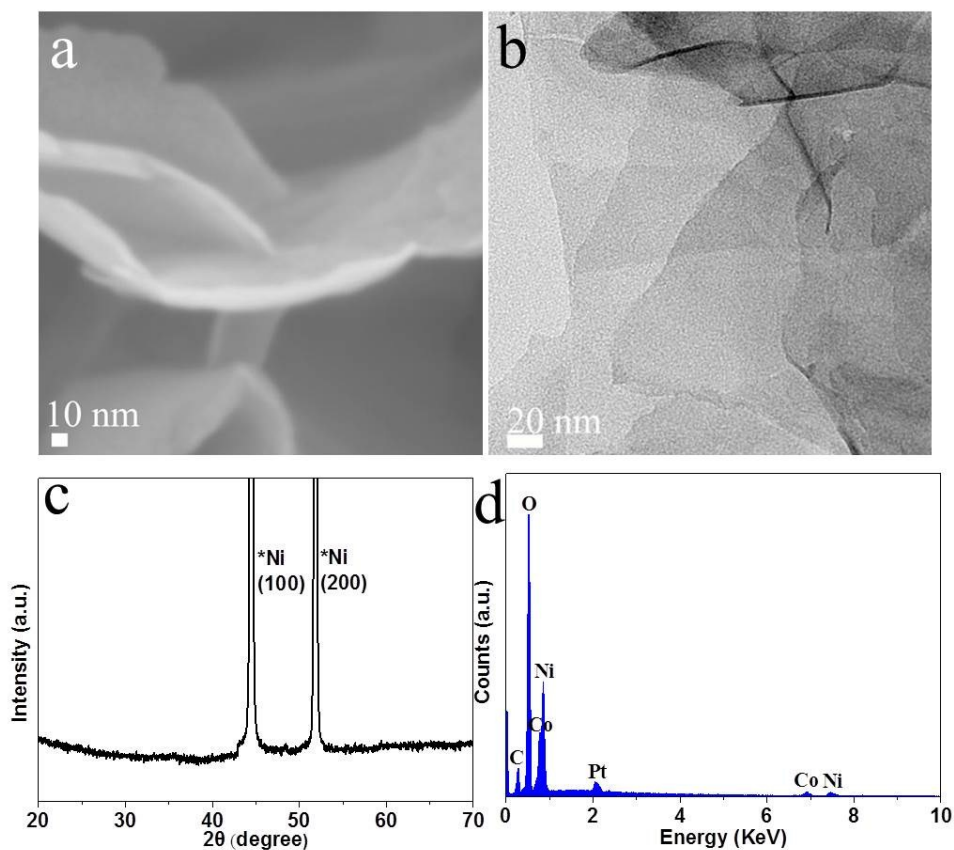
Figure S1. Structure and morphology characterizations of as-fabricated (Co, Ni)(OH)$_2$. (a) high-resolution SEM image, (b) high-resolution TEM image, (c) XRD pattern and (d) EDS.

The XRD pattern exhibits no obvious diffraction peaks except metal Ni, which indicates the amorphous nature of the as-fabricated (Co, Ni)(OH)$_2$. In addition, EDS spectra demonstrate the sample is composed of Co, Ni and O elements.
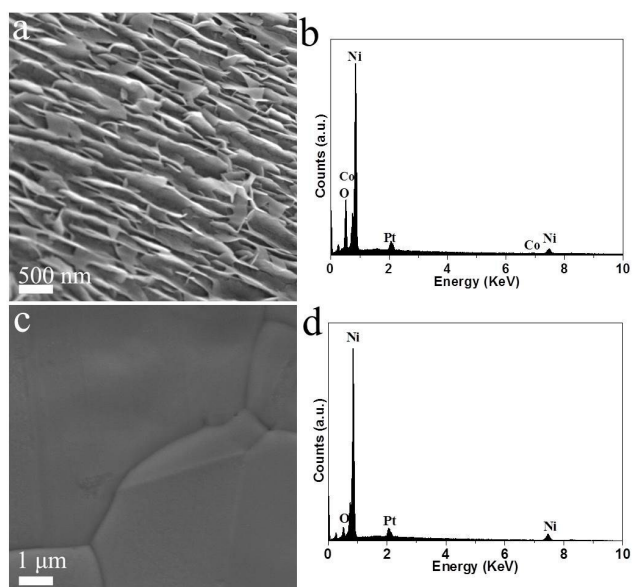
Figure S2. SEM images and the corresponding EDX spectra of materials obtained from attempted synthesis of (Co, Ni)$_3$S$_2$ under the condition (a, b) without Na$_2$SO$_4$ and (c, d) without frist Ni-Co

precursors synthesis step but the other reaction parameters were kept unchanged.
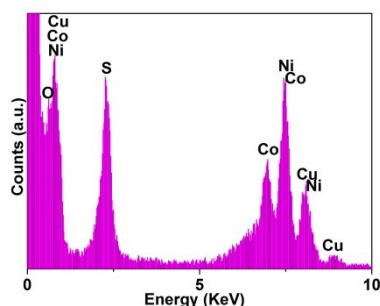
Figure S3. EDS spectra of H-(Co, Ni)$_3$S$_2$.

Table S1

The atomic ratios of Co:Ni:S in (Co, Ni)$_3$S$_2$ and H-(Co, Ni)$_3$S$_2$ electrode materials determined by EDS and ICP-OES.

|	EDS result	ICP-OES result
(Co, Ni)$_3$S$_2$	18.4:42:39.6	18.7:41.8:39.5
H-(Co, Ni)$_3$S$_2$	19:43.5:37.5	19.1:43.6:37.3
alkali solution		10.2:21.7:68.1

The Co:Ni ratio of the as-fabricated (Co, Ni)$_3$S$_2$ honeycomb frameworks are lower than its feeding ratio (1:1) which can be attributed to the lower solubility constant (K$_{sp}$) of Ni(OH)$_2$ than that of Co(OH)$_2$. [1]
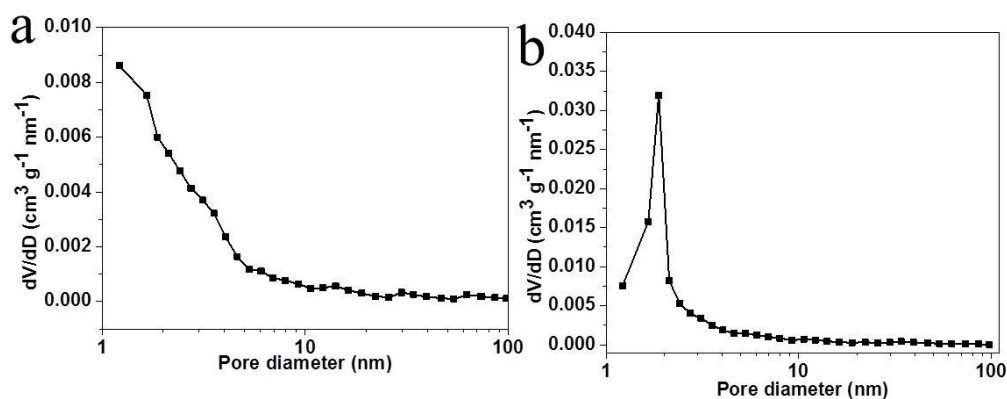
Figure S4. BJH pore-size distribution curve of (a) (Co, Ni)$_3$S$_2$ and (b) H-(Co, Ni)$_3$S$_2$, respectively. The H-(Co, Ni)$_3$S$_2$ shows a more dominant pore size distribution in the range of 1-3 nm than that of (Co, Ni)$_3$S$_2$ calculated by Barrett-Joyner-Halenda (BJH) method, which can be attribute to the micropores in plane of H-(Co, Ni)$_3$S$_2$ after KOH treatment.
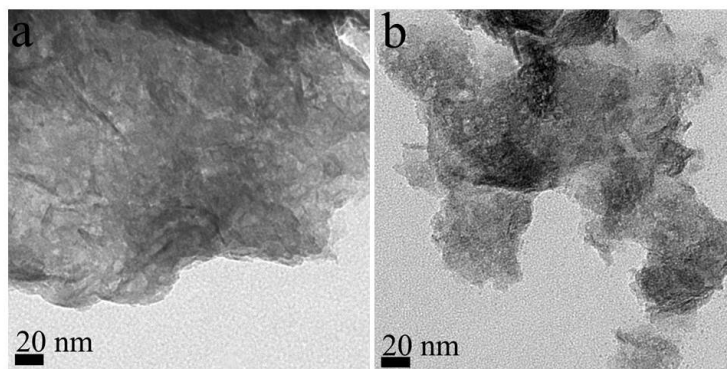
Figure S5. TEM images of the resulting solutions under different reaction temperature during the preparation of H-(Co, Ni)$_3$S$_2$. (a) 60 °C and (b) 100 °C.
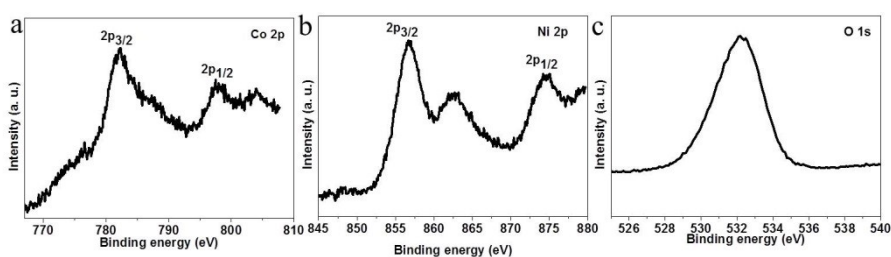

Figure S6. XPS analysis of (Co, Ni)(OH)$_2$. (a) Co 2p, (b) Ni 2p and (c) O 1s.

Figure S6 shows Co, Ni and O element in (Co, Ni)(OH)$_2$. Compared with (Co, Ni)$_3$S$_2$, the Co 2p peaks and Ni 2p peaks exhibit only the corresponding characteristic peaks of the Ni and Co oxides, respectively, without any metallic characteristic peaks, suggesting the different valence states of Co and Ni exist in (Co, Ni)$_3$S$_2$.
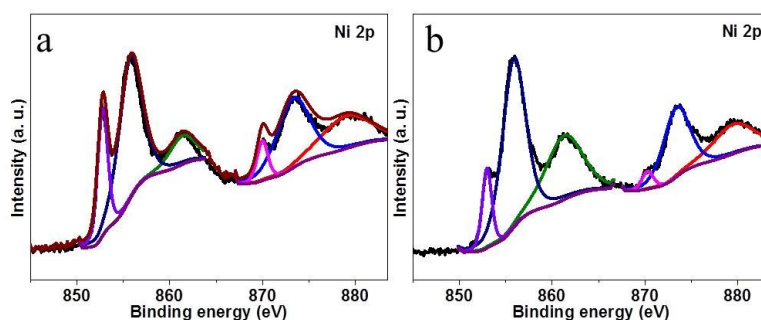

Figure S7. (a) Fitted Ni 2p for pristine (Co, Ni)$_3$S$_2$ and(b) for H-(Co, Ni)$_3$S$_2$.

Compared with (Co, Ni)$_3$S$_2$, H-(Co, Ni)$_3$S$_2$ shows decreased relative intensity ratios of metallic states to divalent states in Co 2p and Ni 2p XPS spectrum, suggesting that the increased divalent states ratio in H-(Co, Ni)$_3$S$_2$. By fitting fine-scanned Ni 2p spectra of both pristine and H-(Co, Ni)$_3$S$_2$ to further investigate the electronic states of Ni atoms with different valences. It can be clearly observed that the atomic ratio of Ni$^{\delta+}$ states to oxidized states (0.4) for H-(Co, Ni)$_3$S$_2$ is higher than that (0.2) of pristine (Co, Ni)$_3$S$_2$ by comparing the area that the fitted curve covered, implying that the increased disorder degree of H-(Co, Ni)$_3$S$_2$ structure and the existence of surface oxides, which can be confirmed by the slightly increase of surface oxygen ratio in XPS spectra.
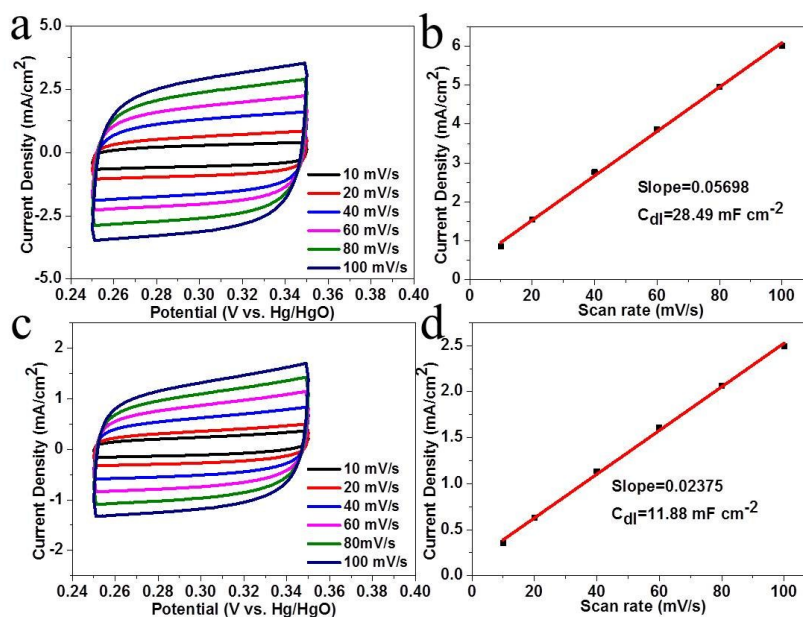
Figure S8. CV curves and linear fit of current densities at 0.3 V versus scan rates for determination the capacitance of double layer (C_{dl}) of (a, b) H-$(Co, Ni)_3S_2$, (c, d) as-prepared $(Co, Ni)_3S_2$.

Electrochemical active surface area (ECSA) is determined by measuring the capacitive current associated with double layer charging from the scan-rate dependence of cyclic voltammetry (CV). By plotting the difference in current density (J) between anodic and cathodic sweeps (ΔJ) at a fixed potential against the scan rate, a linear trend is observed. The fitting slope is twice of the double-layer capacitance (C_{dl}), which is linearly promotional to the ECSA. These values of C_{dl} permit comparison of relative surface activity of different electrodes particularly in same electrolyte. To determine C_{dl} for various electrodes, the potential window of CVs is 0.25 V-0.35V vs. saturated Hg/HgO with the scan rates from 10 mV/s-100 mV/s. The ECSA of 28.49 mF cm^{-2} for holey (Co, Ni)$_3$S$_2$ is two times higher than that of as-prepared (Co, Ni)$_3$S$_2$ (11.88 mF cm^{-2}), suggesting holey (Co, Ni)$_3$S$_2$ provided a larger active area.
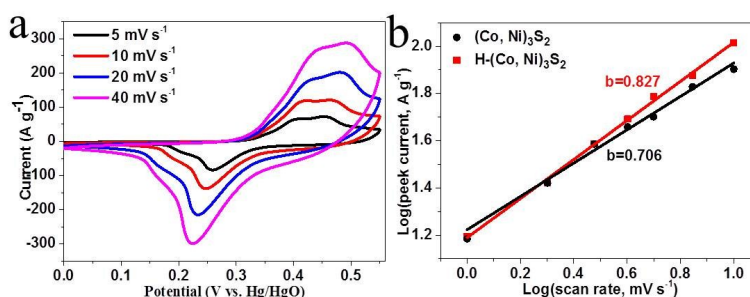

Figure S9. Electrochemical performances of H-(Co, Ni)$_3$S$_2$ electrodes. (a) CV curves at different scan rates, and (b) log (anodic peak current) versus log (scan rate) plot.
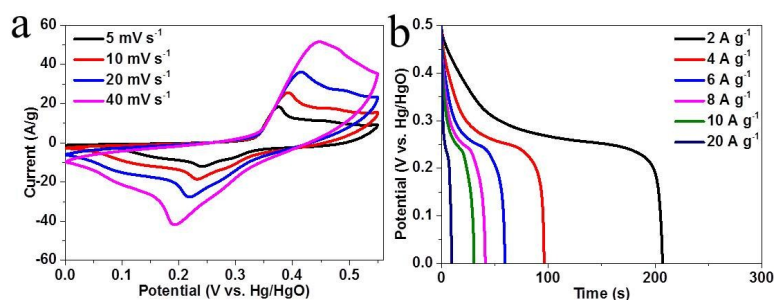
Figure S10. Electrochemical performances of (Co, Ni)(OH)$_2$ electrodes. (a) CV curves at different scan rates, and (b) galvanostatic charge-discharge curves at different current densities.
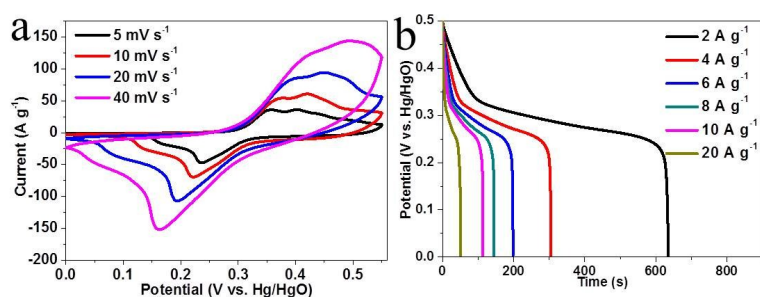
Figure S11. Electrochemical performances of (Co, Ni)$_3$S$_2$ electrodes. (a) CV curves at different scan rates, and (b) galvanostatic charge-discharge curves at different current densities.
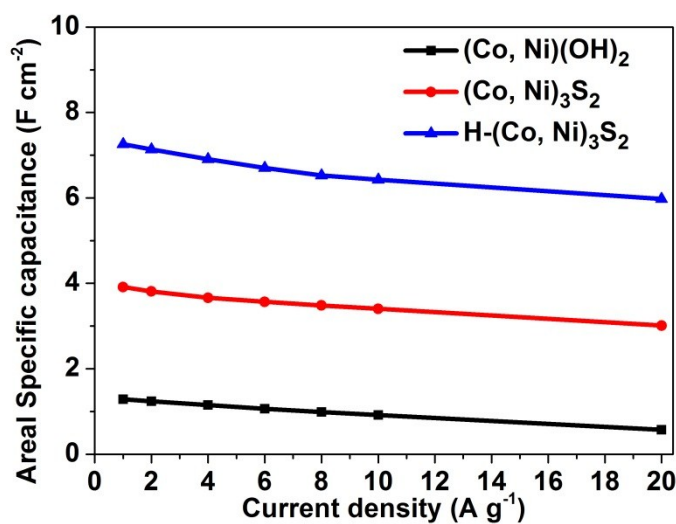
Figure S12. Areal specific capacitances of as-fabricated (Co, Ni)(OH)$_2$, (Co, Ni)$_3$S$_2$ and H-(Co, Ni)$_3$S$_2$ electrodes at current densities from 1 to 20 A g^{-1}, respectively.

Calculation of the Theoretical Capacitances:

According to the faradaic reactions of (5-7), the theoretically available maximum

capacitances of Ni_3S_2 and Co_3S_2 are 2442 F g^{-1} and 4869 F g^{-1} under the bias of 0.5 V.

The estimations are as follows:

Ni_3S_2: [Avogadro constant (6.023 × 10^{23} per mol)] × [1 Ni_3S_2 per mol] × [3 electron per Ni_3S_2] × [1.623 × 10^{-19} C per electron] / [240.19 g per 1 mol of Ni_3S_2] / [0.5 V] = 2442 F g^{-1} for Ni_3S_2;

Co_3S_2: [Avogadro constant (6.023 × 10^{23} per mol)] × [1 Co_3S_2 per mol] × [6 electron per Co_3S_2] × [1.623 × 10^{-19} C per electron] / [240.92 g per 1 mol of Co_3S_2] / [0.5 V] = 4869 F g^{-1} for Co_3S_2.